NASA/TM–20250009254

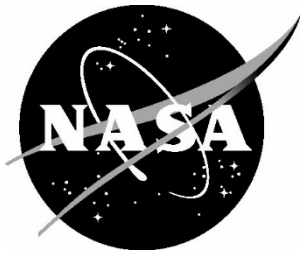

Terrain Maps for Low Altitude Aviation from Commercial Satellite Photogrammetry

Andrew J. Moore
NASA Langley Research Center, Hampton, VA

J. Sloan Glover
Analytical Mechanics Associates, Inc., Hampton, VA

Andrew Turner
ViGYAN, Inc., Hampton, VA

September 2025

NASA STI Program Report Series

Since its founding, NASA has been dedicated to the advancement of aeronautics and space science. The NASA scientific and technical information (STI) program plays a key part in helping NASA maintain this important role.

The NASA STI program operates under the auspices of the Agency Chief Information Officer. It collects, organizes, provides for archiving, and disseminates NASA's STI. The NASA STI program provides access to the NTRS Registered and its public interface, the NASA Technical Reports Server, thus providing one of the largest collections of aeronautical and space science STI in the world. Results are published in both non-NASA channels and by NASA in the NASA STI Report Series, which includes the following report types:

- TECHNICAL PUBLICATION. Reports of completed research or a major significant phase of research that present the results of NASA Programs and include extensive data or theoretical analysis. Includes compilations of significant scientific and technical data and information deemed to be of continuing reference value. NASA counterpart of peer-reviewed formal professional papers but has less stringent limitations on manuscript length and extent of graphic presentations.

- TECHNICAL MEMORANDUM. Scientific and technical findings that are preliminary or of specialized interest, e.g., quick release reports, working papers, and bibliographies that contain minimal annotation. Does not contain extensive analysis.

- CONTRACTOR REPORT. Scientific and technical findings by NASA-sponsored contractors and grantees.

- CONFERENCE PUBLICATION. Collected papers from scientific and technical conferences, symposia, seminars, or other meetings sponsored or co-sponsored by NASA.

- SPECIAL PUBLICATION. Scientific, technical, or historical information from NASA programs, projects, and missions, often concerned with subjects having substantial public interest.

- TECHNICAL TRANSLATION. English-language translations of foreign scientific and technical material pertinent to NASA's mission.

Specialized services also include organizing and publishing research results, distributing specialized research announcements and feeds, providing information desk and personal search support, and enabling data exchange services.

For more information about the NASA STI program, see the following:

- Access the NASA STI program home page at http://www.sti.nasa.gov

- Help desk contact information: https://www.sti.nasa.gov/sti-contact-form/ and select the "General" help request type.

NASA/TM–20250009254

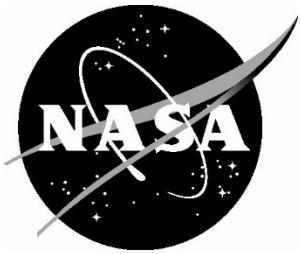

Terrain Maps for Low Altitude Aviation from Commercial Satellite Photogrammetry

Andrew J. Moore
NASA Langley Research Center, Hampton, VA

J. Sloan Glover
Analytical Mechanics Associates, Inc., Hampton, VA

Andrew Turner
ViGYAN, Inc., Hampton, VA

National Aeronautics and
Space Administration

Langley Research Center
Hampton, Virginia 23681-2199

September 2025

Available from:

NASA STI Program / Mail Stop 050
NASA Langley Research Center
Hampton, VA 23681-2199

Acknowledgments

The Research and Development described herein was conducted over the course of the System Wide Safety project, part of NASA's Aviation Operations and Safety Program, and would not have been possible without the leadership, support, and sponsorship of NASA's Aeronautics Research Mission Directorate. The authors are grateful to Steve Young, Evan Dill, Misty Davies, and Kyle Ellis for their vision and constancy. They recognized the difficulty and importance of accurate terrain mapping in assuring safety for low-altitude flight. We are grateful to Corey Diebler for the image of the NASA Flight Dynamics Research Facility.

The use of trademarks or names in this report is for accurate reporting and does not constitute an official endorsement, either expressed or implied, of such products or manufacturers by the National Aeronautics and Space Administration.

Map data attributions often contain multiple sources which must be abbreviated in figure citations for space considerations. An appendix is included with all image and map source organizations defined and cited.

Abstract

Safe low-altitude flight operations necessitate accurate terrain mapping capabilities to mitigate multiple operational hazards. This report evaluates an emerging mapping methodology, satellite image photogrammetric mapping, and its applicability to flight safety requirements.

Aerial lidar surveys have historically represented the primary methodology for generating detailed three-dimensional terrain maps. These systems provide exceptional spatial resolution capabilities, typically achieving decimeter-level accuracy that exceeds the meter-level requirements necessary for spatial hazard identification. However, widespread adoption of mapping from aerial lidar surveys is limited by high acquisition costs and data volume management challenges.

Recent developments in commercial satellite imaging have enabled alternative mapping approaches utilizing stereo matching and photogrammetric processing techniques. Compared to maps based on aerial lidar surveys, maps based satellite imagery are less expensive, faster to prepare, easier to distribute, and scalable to wider areas. This report asks two questions. First, do maps based on satellite imagery possess the spatial resolution and accuracy required for flight hazard reduction? Second, are maps based on satellite imagery consistent over time, i.e., do they correctly track changes as the landscape changes?

This report, based on evaluation of a series of four satellite-based maps of a 100 km^2 area acquired at six month intervals over 2 years, concludes that they do meet the required levels of resolution and accuracy needed to identify most, but not all, terrain hazards. For undetected terrain hazards (thin features such as power lines), one approach to supplementing satellite-based maps is described. Further, consistency checks over time found that the 3D features were stable in static regions of the landscape and were reliably updated in regions of the landscape that changed.

1.0 Introduction

1.1 Mapping requirements for safe low-altitude aviation

Conventional aviation relies on regularly updated maps of ground facilities. Complete 3D mapping around airports and runways [1] is mandatory for about 1000 of the larger airports in the USA. The Federal Aviation Administration requires that these maps must be updated every 56 days [2]. However, just as the number of aircraft in the airspace is set to grow due to emerging low-altitude operations, the number of areas that must be mapped will grow as facilities for low-altitude aviation come online.

Low-altitude aviation requires detailed 3D maps to mitigate several safety hazards [3][4]:

- collisions with obstacles,
- poor navigation fidelity,
- ground population impact risk,
- high/turbulent winds, and
- loss of radio connectivity.

Unlike the terrain around conventional airports and runways, the terrain near facilities for low-altitude aviation is generally denser, more varied, and less flat than the flat, open terrain around airport runways. One reason for this terrain difference is that urban air mobility (i.e., air taxis) is a major market driver for low-altitude aviation. More generally, the vertical takeoff and landing capability of many low-altitude aircraft invites a less restrictive operational area than large aircraft with long takeoff and landing glide paths. In addition to three dimensional maps of

buildings and foliage near landing areas (e.g., vertiports) there is a potential need for mapping along low-altitude flight paths so that emergency landing (ditch) sites are well characterized.

Until recently, only aerial lidar could provide such complex 3D maps. Lidar surveys can provide spatial resolution on the order of a decimeter, higher than the meter-level need to chart spatial hazards. Indeed, besides manual surveying, only lidar-based maps have regulatory clearance for conventional airport terrain maps [1]. Aerial lidar mapping is expensive and requires intensive planning to execute at a cadence of 56 days; if the survey site is urban, timely execution is even more difficult. Aerial lidar surveys suffer from another disadvantage: they generate high volumes of data which are burdensome to store, distribute and process.

1.2 Satellite-based mapping as an alternative to lidar

In the last five years, maps created from geometric processing of satellite imagery [5][6][7] (also known as satellite-based photogrammetry or satellite-based mapping) have attained meter-level accuracy and precision.

Compared to lidar-based terrain mapping, satellite-based terrain mapping has cost and availability advantages. After the capital cost of building and launching the satellite fleet, satellite-based mapping costs are low (fleet maintenance, data storage, and computing) compared to the cost of the airplane flight needed for a lidar survey. Since orbital satellites are continually acquiring images, 3D maps constructed from their imagery could conceivably be computed much faster than the current 8-week regulatory refresh rate.

Emerging satellite-based mapping technology is not a panacea. While satellite-based maps have sufficient spatial detail to map buildings and terrain, they cannot fully resolve very thin obstacles such as power lines [8]. (Note that aerial lidar cannot resolve all thin obstacles either [8]). Currently, manual effort is needed in addition to satellite-based photogrammetry to faithfully map this class of hazard, which also includes power lines, street signs, and cables. Human effort is required a) to delineate the hazardous features and then b) to overlay, annotate or otherwise merge the features with the satellite-based terrain map.

This report evaluates a series of 3D maps of a specific 100 km^2 area constructed periodically from satellite imagery. The evaluation tests for two essential measures of quality: consistency and accuracy. To judge consistency, the locations of terrain features are compared across time. To judge accuracy, the locations of real-world terrain features are compared to their locations in other maps.

1.3 Report Organization

The remainder of this report is organized as follows. The area mapped and the map delivery dates are described in Section 2. The digital datatypes delivered in the mapping data are detailed in Section 3. Validation tests of the mapping data are described in Section 4, including comparison against existing maps and comparison across time. Concluding remarks are provided in Section 5.

Map data attributions often contain multiple sources which must be abbreviated in figure citations for space considerations. An Appendix is included with all image and map source abbreviations defined and cited.

2.0 Spatial extent of coverage and delivery dates

2.1 Small-area evaluation data

Satellite-based 3D maps covering a small, square test area (dimensions: 6.2 km^2, approximately 2.5 km on a side) centered on the NASA Langley Research Center were obtained from vendor Maxar Intelligence [9] and evaluated between July and October 2022. The red box in Fig. 2.1 (left) shows the location of the evaluation data, and Fig. 3.1.1 shows its ground terrain (left) and above-ground features (right). The evaluation data met all functional criteria, and so four sets of wide-area satellite-based 3D maps gathered in successive six month periods were purchased.

2.2 Wide-area data

Each wide-area map covered a 100 square kilometer area in southeast Virginia (Fig. 2.1, left) stretching roughly from NASA Langley Research Center in the north to Fort Monroe in the south. Image collection was repeated every 6 months for a period of 2 years. Fig. 2.1, right, shows a perspective view of the terrain map rendered as a set of green foliage geometries and blue building geometries.

Image collection, processing, and delivery were as follows (Table 1). The vendor satellite fleet collected images over a six month period up to one month prior to each delivery. In the following month, the vendor computed the 3D geometry and created the map datatypes described in Section 3. Delivery to NASA followed immediately thereafter.

Table 1. Wide-area image collection, processing, and delivery

Delivery Number	Delivery Date	Satellite Tasking Window[1]	
		Start	End
1	March 31, 2023	September 1, 2022	February 28, 2023
2	September 30, 2023	March 1, 2023	August 30, 2023
3	March 31, 2024	September 1, 2023	February 29, 2024
4	September 30, 2024	March 1, 2024	August 30, 2024

[1] 'Tasking window' refers to image acquisition by the satellite fleet for terrain updates. In unchanged areas of the terrain map, imagery collected prior to the tasking window was also used to construct the 3D geodata. The oldest images used for construction were collected in January 2021.

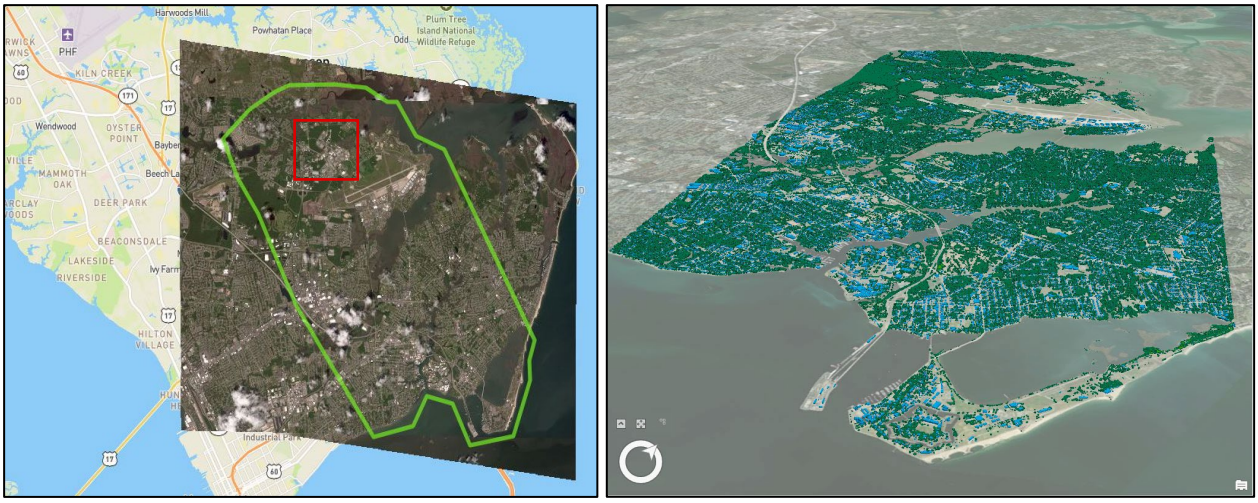

Fig. 2.1. Left: Spatial extent of 100 km^2 mapping area (green contour) drawn on superimposed satellite and street maps. The evaluation area is also shown (red contour). Right: Perspective view from south-southeast with foliage colored green and buildings colored blue. *Left image sources: basemap OpenStreetMap , imagery © 2023 Maxar Technologies. Right image sources: terrain © 2023 Maxar Technologies, basemap Maxar via ESRI/ArcGIS.*

3.0 Delivered geometries

Three dimensional terrain data were delivered in three forms:

- Bare-earth ground terrain (geoTiff) geometry
- Vector (shape file) geometry
- Point cloud (pseudo Lidar) geometry

All forms of geodata used the same geographic coordinate system: horizontal (longitude and latitude) coordinates used the WGS 84 / UTM 18N (World Geodetic System/Universal Transverse Mercator zone 18) system [10][11] and vertical (altitude) coordinates were expressed in meters above the EGM2008 (Earth Gravitational Model 2008) geoid [12].

3.1 Bare-earth ground terrain geometry

A Digital Terrain Model (DTM), i.e., a bare-earth ground terrain, was delivered as a set of files in the geoTiff format. The altitude at each location of the DTM was represented as a grayscale value (Fig. 3.1.1 left). Each file was 4 km on a side, so that 12 files sufficed to tile the 100 km^2 area.

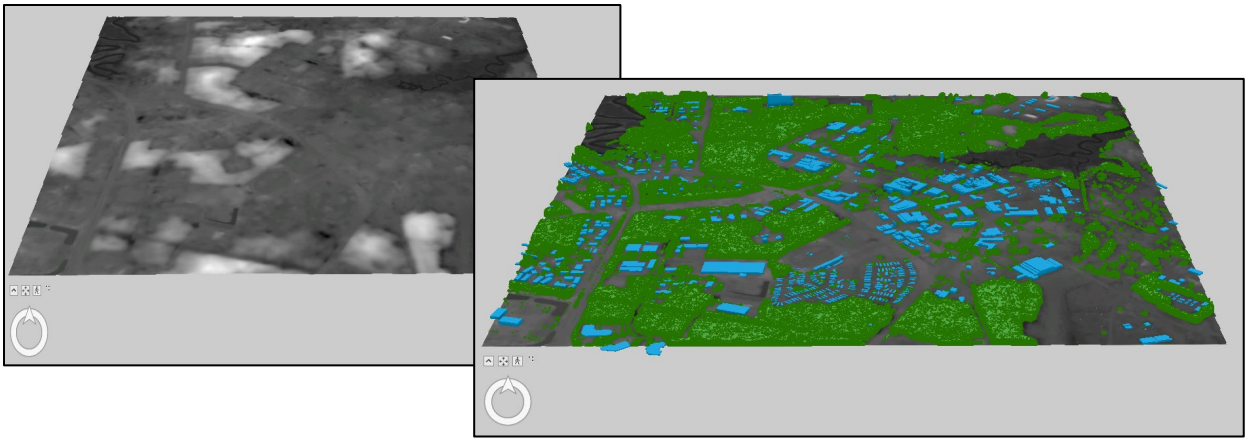

Fig. 3.1.1. Left: Bare-earth map of 6.2 km^2 test area containing the NASA Langley Research Center. In this Digital Terrain Model (DTM), altitude is rendered as grayscale variation in a flat geoTiff format. Right: Foliage (green) and building (blue) features represented as vector shapes, overlaid on the DTM to form a Digital Surface Model (DSM). *Image sources: © 2022 Maxar Technologies.*

3.2 Vector (shape file) geometry

Terrain features in vector shape files were separated by the vendor into foliage and building data sets. A foliage feature was represented as a set of right polyhedra (perpendicular to ground and extruded to a maximum elevation) with the lowest-elevation polyhedron enclosing the next-lowest, etc. (Fig. 3.2.1, left). This may be regarded as a '2.5D polyhedral construction' (see Fig.

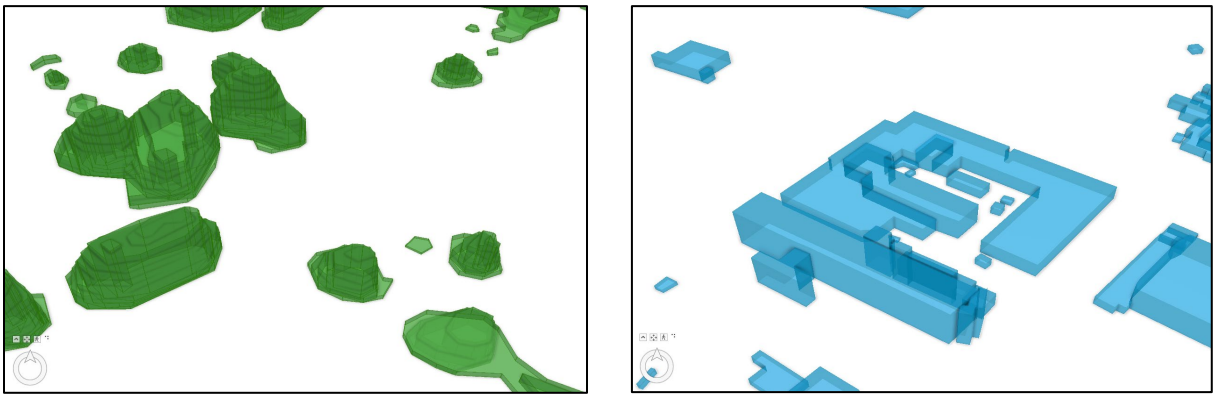

Fig. 3.2.1. Vector DSM constructed of 2.5D right polyhedra. Transparent colors are used here to reveal the construction foliage (left) and building (right) feature geometry. *Image sources: © 2022 Maxar Technologies.*

1 of [8]). The set appeared as a terraced (stacked) set of layers with one meter altitude terracing. Extrusion height of each element of the foliage construction was enumerated as meters AGL (above ground level), so that a DTM ground reference was needed to compute absolute altitude.

Similarly, building features (Fig. 3.2.1, right) were represented as sets of enclosing right polyhedra. The terracing visual effect was not as evident as for foliage, since building height variation is not gradual. The extrusion height of each element of the building construction was enumerated both as meters AGL and as height above ellipsoid, so that absolute altitude could be determined with or without a DTM ground reference.

Both foliage and building vector features are shown in Fig. 3.2.2 at one location within the mapping region, the Hampton University campus (76.3392516°W 37.0205623°N). The features are overlaid on an aerial photo of the region, and the correspondence between vector features and the terrain imaged in the aerial photo appears to be very close.

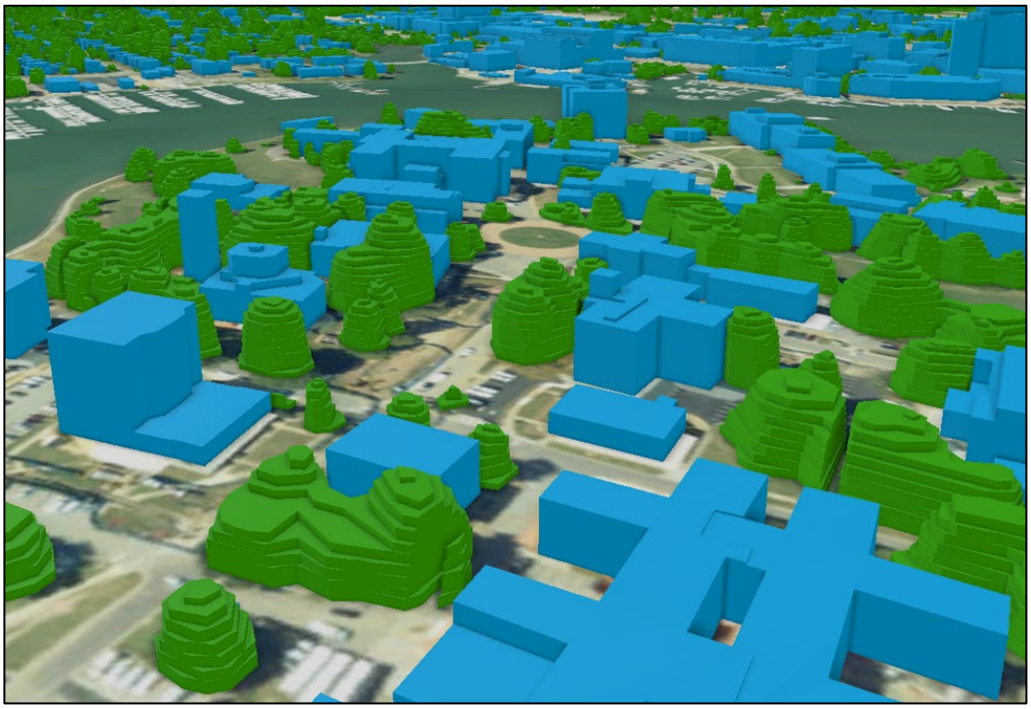

Fig. 3.2.2. Close-up view of 3D satellite-based map of Hampton University with foliage colored green and buildings colored blue. *Image sources: 3D features © 2022 Maxar Technologies; basemap source Esri, HERE, Garmin, OpenStreetMap.*

3.3 Point cloud geometry

Point cloud files were not separated by the vendor into foliage and building data sets; it was necessary to find building footprints (via ground projection of the shapefiles) to segregate building points, and to exclude those from the point cloud to segregate foliage points. The pseudo-lidar point clouds represented only the topmost surface, as if they were points on a cloth draped over the top of the terrain (Fig. 3.3.1, right). Since point cloud altitude was delivered as meters AGL, the ground terrain (DTM) data was needed to compute the point-wise absolute altitude of the separated foliage and building point cloud datasets.

Lidar was organized as a set of rectangular tiles of extents up to 1.5 km by 1.5 km (Fig. 3.3.2 left) colorized with the overhead image view (Fig. 3.3.2 right). Each delivered dataset contained a total of 61 point cloud tiles; since the wide-area 100 km^2 area was somewhat irregular and not aligned with the cardinal directions, about one third of the tiles were smaller than the maximum 2.25 km^2 size.

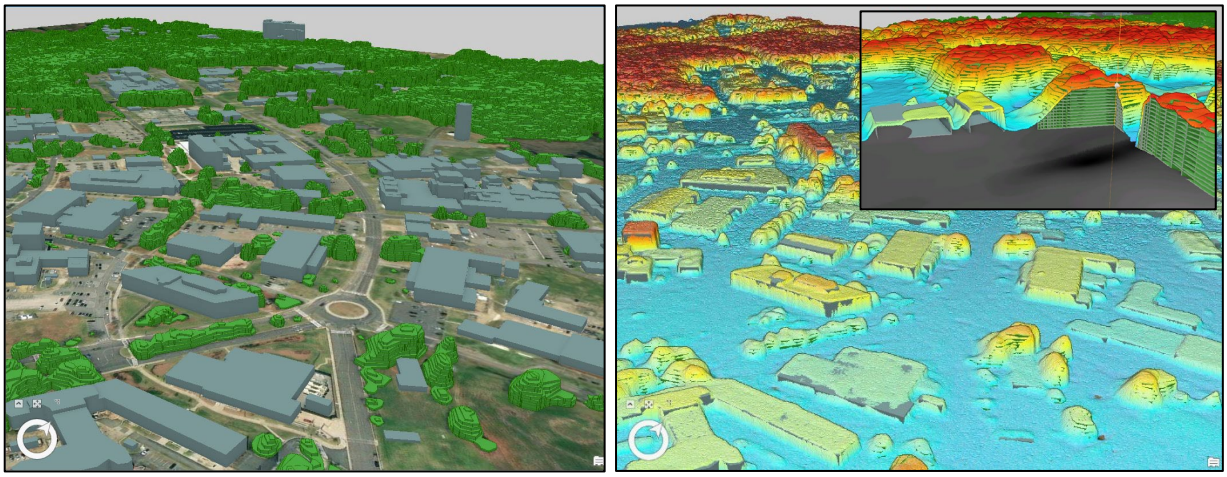

Fig. 3.3.1. Left: Vector DSM (green foliage and grey building) overlaid on a DTM colored with a top-down view for an area the NASA Langley Research Center. Right: Point cloud overlaid with vector image elements and rendered with a blue-to-red elevation color scale. The point cloud, unlike traditional lidar obtained from overflights with a downward-directed laser, does not penetrate the foliage canopy. Instead, it samples the topmost elevation at each location, like a cloth draped over the DSM. Inset: a vertical cross section shows tight vertical point cloud layer alignment and with some lateral smoothing at the edges of features. *Left image source: 3D features © 2022 Maxar Technologies; basemap source Esri, HERE, Garmin, OpenStreetMap. Right image sources: © 2022 Maxar Technologies*

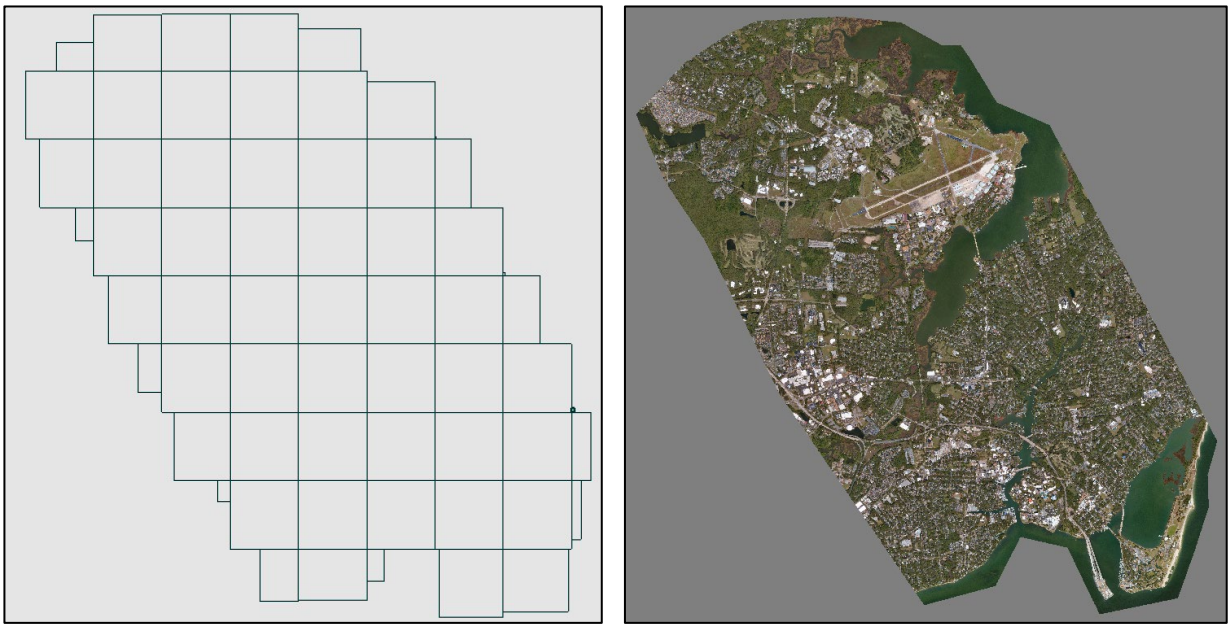

Fig. 3.3.2. Left: The 100 km^2 point cloud map area was partitioned into spatial tiles of size 2.25 km^2 or less. Right: Point clouds were colorized with spatially registered top-down imagery. *Image sources: © 2023 Maxar Technologies.*

3.4 Geometric level of detail and storage requirements

3.4.1 Geodata level of detail

Ground terrain (DTM) data was delivered as GeoTiff with sampling distance (post spacing) of 50 cm, and post placement absolute accuracy of 3 m LE90 (90th percentile linear error) and 3 m CE90 (90th percentile radial error) [13]. The relative (post-to-post) accuracy was 1 m LE90 and 1 m CE90.

The features in vector (shape) format had a point spacing of 50 cm and nominal accuracies [14][15] specified as follows. 1) Lateral (X-Y or longitude-latitude) positional accuracy is +/- 3 m for the building centroid. 2) Vertical accuracy both in absolute height (MSL, or height above mean sea level) and in height relative to ground (AGL) is +/- 3 m.

The features in point cloud (LAS) format had a point spacing of 50 cm, and nominal [16] absolute lateral accuracies of 3 m SE90 (90th percentile spherical error), 3 m LE90, and 3 m CE90, and a relative lateral accuracy (i.e., between nearby points) of 1 m SE90, 1 m LE90, and 1 m CE90.

3.4.2 Storage requirements

The storage size for the three forms of geodata for the 100 km^2 area is given in Table 2. The ground DTM in geoTiff format requires 635 MB of disk storage. The feature datatype is most efficiently represented in vector (Shape) format, requiring 100 MB of storage, while features in LAS point cloud format require 8.5 GB of storage, almost two orders of magnitude more than the vector representation.

Table 2. Storage by datatype

Geometry type	Storage for 100 km^2 area
Bare-earth ground terrain	635 MB
Vector (shape file) features	100 MB
Point cloud (pseudo Lidar) features	8.5 GB

4 Validation

The 3D satellite-based maps from the evaluation dataset and the four wide-scale datasets were tested for two essential measures of quality, accuracy and consistency. Accuracy was assessed by measuring the locations of real-world terrain features compared to their locations in other maps, and checking whether the location differences were within the specified nominal accuracy. Consistency was assessed by comparing the locations of terrain features across time, i.e., across separate datasets. Some landscape features changed (due to construction or demolition) during the six month intervals between datasets, and the appearance or disappearance of those features was checked also. The data met or exceeded the expected accuracy and consistency checks as detailed below.

4.1 Validation of Accuracy

4.1.1 Reference Maps Utilized

Reference maps were chosen to test the accuracy of geometry in the small (10 km^2) evaluation area centered on the NASA Langley Research Center. The reference maps are:

1) Google Earth imagery [17]
2) ArcGIS World Imagery and World Imagery Hybrid basemaps [18]
3) Bing maps imagery [19]
4) Three representations of a February 2018 aerial lidar survey of a 1.0 square mile (2.59 km^2) area centered on the NASA Langley Research Center:
    a. raw survey data in LAS (LASer) point cloud file format with an average point spacing of 0.1m,
    b. building and foliage ground footprints, hand drawn to circumscribe the points from the point cloud corresponding to the feature, and
    c. vector (shape) files derived from the ground footprints extruded to the height of the corresponding subset of the point clouds. (2.5D)

    This dataset was extensively validated with manual surveys by the NASA Langley GIS group. Reference [8] shows details of this dataset, including the footprint and extruded (2.5D) forms derived from the point cloud.

The accuracy of terrain features mapping in all delivered datatypes was first checked extensively against reference maps in the small-area evaluation data, and then checked at a few points in the wide-area evaluation data. The initial focus on the small-area data allowed for

a) development of measurement techniques appropriate to the data type and reference maps,
b) consistency cross-checks between reference maps,
c) extensive use of the most-trusted reference, the LaRC lidar survey.

All four reference maps were consistent within 1 m laterally and vertically.

DTM. In the small-area evaluation data, both the absolute and relative DTM accuracy metrics (3 m and 1 m, respectively) claimed in the vendor datasheet [13] were verified by comparison against all four reference maps (listed in Section 4.1.1.) at several dozen points free of buildings and foliage. In the wide-area evaluation data, both the absolute and relative DTM accuracy metrics were verified by comparison against two reference maps (Google Earth and ArcGIS) at 5-10 points free of buildings and foliage. Altitude accuracy at 5-10 points was within 1 m of the reference maps.

Vector. The lateral accuracy of vector representations of building features was specified as building centroid placement accuracy [14][15], which is difficult to verify by direct measurement. Instead, lateral boundary accuracy was checked. Building edge placement accuracy was typically +/- 1 m against all four reference maps at several dozen points within the small-area evaluation data, and never worse than the specified +/- 3 m accuracy. In the wide-area evaluation data, inspection of 5-10 diverse structures also showed typical building edge placement accuracy of +/- 1 m.

Building vertical accuracy was also +/- 1 m at these points. For buildings, there is an important caveat that must be mentioned regarding building vertical accuracy: as specified [14][15], structures with footprints smaller than 7 m × 7 m in size were not always resolved. Building rooftops frequently have features such as HVAC equipment with footprints smaller than this. Vertical comparison between the delivered data and reference maps was performed only in broad, flat rooftop areas.

For foliage geodata, only lateral accuracy was verified due to the inherent ambiguity in bounding the tops of trees [8]; the delivered foliage geodata met or exceeded the specified accuracy at several diverse points[2].

[2] The 2018 lidar survey (item 4 in Section 4.1.1) was not used for this measurement, since foliage growth in the four years between maps could exceed one meter.

Point cloud. Accuracy of the point cloud data was not measured explicitly. This is because the point cloud closely followed the vector feature representation as shown in Fig. 3.3.1. Spot checks were performed during the vector accuracy checks to verify the vertical coincidence of vector features and point cloud points; in all cases, tight coincidence similar to Fig. 3.3.1 was found.

4.2 Validation of Consistency

4.2.1 Processing for image change detection

For a 100 km^2 area, it is not practical to search for landscape changes by comparing maps at the individual city block or building level. A Boolean XOR (exclusive OR) operation on pairs of vector layers profoundly highlights differences between the layers, and enables rapid visual comparison is possible via , which highlights differences . This is illustrated in Fig. in 4.2.1.1, which shows changes over a 6 month period in building and foliage[3].

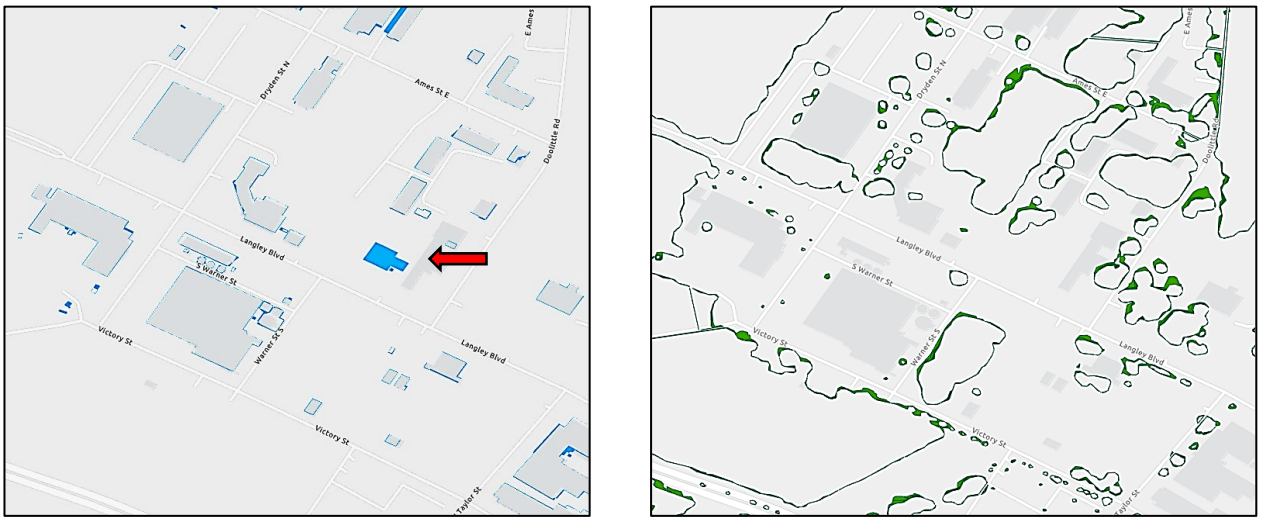

Fig 4.2.1.1 Top-down view of pairwise XOR of building layers (blue, left) and tree layers (green, right) to reveal differences across the time between the first two geodata deliveries. The XOR results are overlaid on a basemap with street names. Only thin (less than one meter) differences are seen for most buildings, which demonstrates meter-level placement consistency. Construction started on a new wind tunnel (the NASA Flight Dynamics Research Facility) in the time between map deliveries; this new structure is the solid blue shape at center left (red arrow). Tree and shrubbery growth in the spring and summer are revealed in the foliage XOR at right. The horizontal length of both images is approximately 650 m. *Image feature sources: NASA from features ©2023 Maxar Technologies. Base map sources: Base map sources: VGIN, Esri, TomTom, Garmin, SafeGraph, GeoTechnologies, Inc, METI/NASA, USGS, EPA, NPS, US Census Bureau, USDA, USFWS.*

XOR outputs are overlaid on the ArcGIS “Light Gray Base” basemap in Fig. 4.2.1.1. Landscape features that did not change in the 6 month period are reduced to a thin ‘difference border’ that reflects slight placement differences from one map to the other, while new construction appears as a solid area. The ‘difference borders’ of buildings are thin (less than 3 m in thickness) as per the vendor accuracy specification.

[3] The “Symmetrical Difference” geoprocessing operation in the ArcGIS Pro tool was used to accomplish the XOR. In this example, map layers from delivery 1 and delivery 2 are processed, so that landscape changes between February 28, 2023 and August 30, 2023 are highlighted.

A further advantage of this technique is that visual comparison of the XOR difference to the basemap provides an approximate supplemental check to the measurements detailed in Section 4.1. The 'difference borders' of buildings should align with the base map features within +/- 3 m. If there is not alignment, a detailed comparison with one or more additional reference maps is warranted. (This alignment is only approximate though, since the mapping time and geometric accuracy of basemaps can vary).

In the remainder of this section, select landscape changes detected with this method are shown following deliveries 2 through 4, and in some instances independent evidence of the terrain is described which validate the map changes.

4.2.2 Difference from second delivery to first delivery

After receipt of the second map dataset, XOR comparisons were performed against the first map dataset to detect landscape changes from March to September 2023. Fig. 4.2.2.1 shows the building (blue) and foliage (green) XOR outputs for the entire 100 km^2 at left, and those outputs overlaid on the ArcGIS "Light Gray Base" for the northern half of the mapping area at right. In the right image, three features with solid color are highlighted with arrows: the wind tunnel new construction site of Fig. 4.2.1.1 (red arow); a clear cut area of a construction site

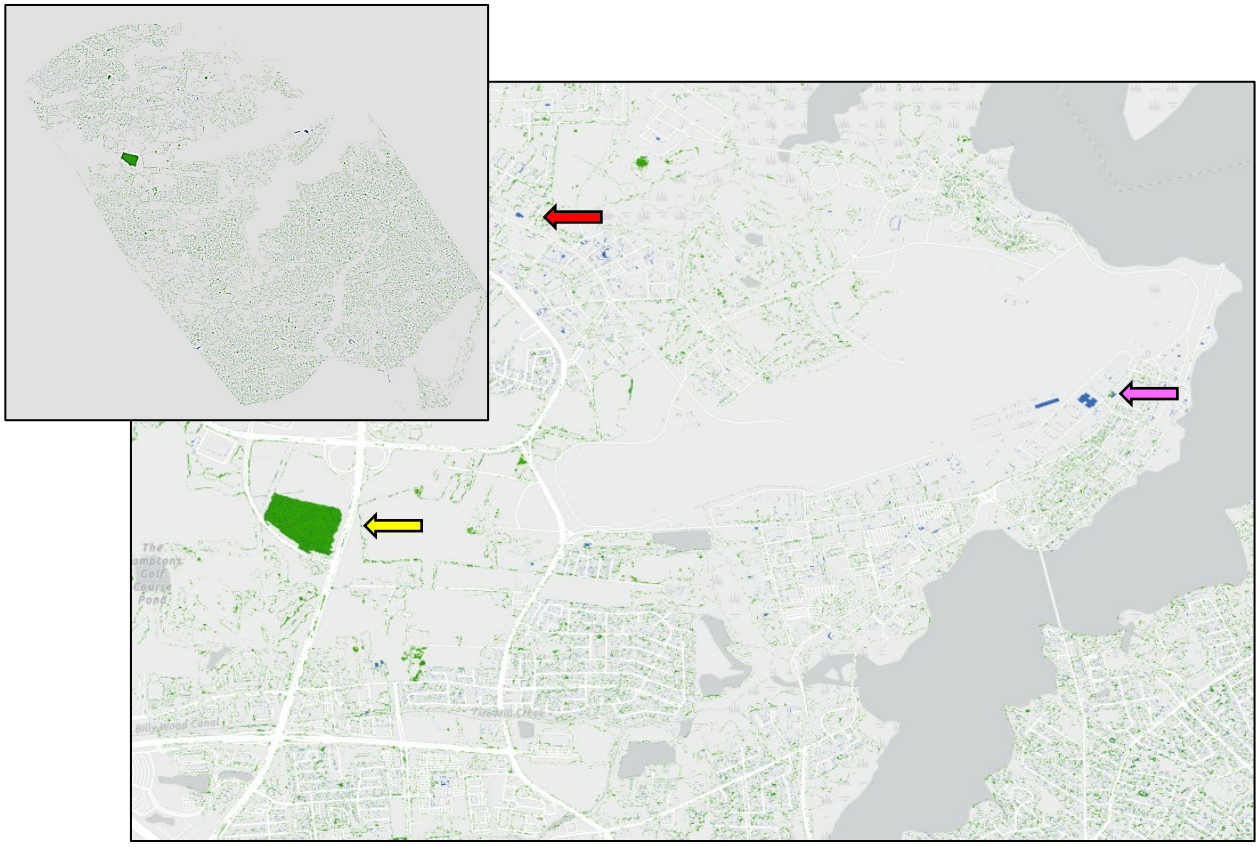

Fig 4.2.2.1. Left inset: Difference map of the 100 km^2 area comparing March to September 2023, with buildings in blue and foliage in green. Right: Enlargement of top half of mapping area. The wind tunnel construction of Fig. 4.2.1.1 is visible at top (red arow). A clear cut area of a construction site is visible at left (yellow arrow). The sites of buildings demolished adjacent to the runway at Langley Air Force Base are visible at right (pink arrow). The horizontal length of the images are: 13 km (left), 7 km (right).

Image feature sources: NASA from features ©2023 Maxar Technologies. Base map sources: VGIN, Esri, TomTom, Garmin, SafeGraph, GeoTechnologies, Inc. METI/NASA, USGS, EPA, NPS, US Census Bureau, USDA, USFWS.

(yellow arrow); and, the sites of demolished buildings adjacent to the runway at Langley Air Force Base (pink arrow). The first 2 were verified by driving to the sites, and the third was verified using Google Earth historical map data.

4.2.3 Difference from third delivery to prior deliveries

After receipt of the third map dataset, XOR comparisons were performed against the first and second map datasets to detect landscape changes from March 2023 to September 2023 and from March 2023 to March 2024. Fig. 4.2.3.1 shows the March-to-September building XOR outputs for an area centered on downtown Hampton Virginia. Besides grading changes at Hampton University's Armstrong Stadium (yellow arrow), construction is evident at middle left (red arrow). The latter was verified using Google Earth historical map data (right inset of Fig. 4.2.3.1). Fig. 4.2.3.2 shows March-to-March (2023 to 2024) foliage XOR outputs across the 100 km2 area. Besides minor foliage changes presumably due to growth, the clear-cut area noted above is visible (pink arrow). Signage at the site revealed that a distribution center was under construction (right inset of Fig. 4.2.3.2).

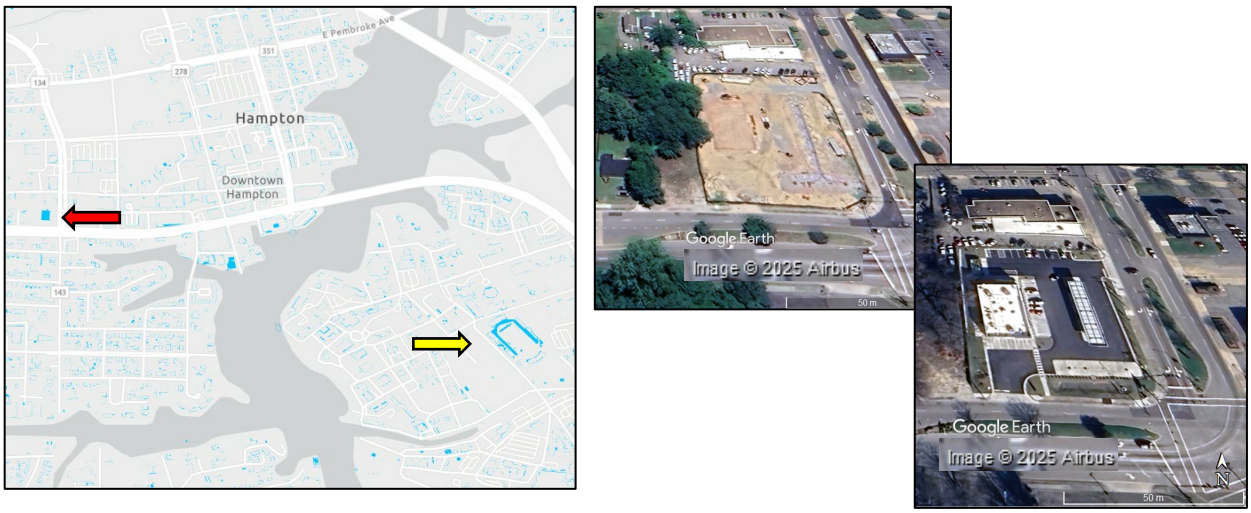

Fig. 4.2.3.1 Select building differences from second delivery (September 2023) to third delivery (April 2024). Left: XOR outputs for an area centered on downtown Hampton Virginia showing new construction (red arrow) and grading at Hampton University's Armstrong Stadium. Right: Google Earth historical imagery from June 2023 (top) and February 2024 (bottom) showing construction of 7-Eleven.

Left image feature sources: NASA from features ©2023, 2024 Maxar Technologies. Left image base map sources: VGIN, Esri, TomTom, Garmin, SafeGraph, GeoTechnologies, Inc, METI/NASA, USGS, EPA, NPS, US Census Bureau, USDA, USFWS. Right image sources: Google Earth, Image 2025 © Airbus

Fig. 4.2.3.2 Left: Foliage differences from April 2023 to April 2024 across entire 100 km^2 swath. Except the clear cut area (pink arrow) described above, differences are likely due to organic growth. Inset right: signage at distribution building construction site with clear cut visible in background.
Left image feature sources: NASA from features ©2023, 2024 Maxar Technologies. Left image base map sources: VGIN, Esri, TomTom, Garmin, SafeGraph, GeoTechnologies, Inc, METI/NASA, USGS, EPA, NPS, US Census Bureau, USDA, USFWS. Right image source: NASA (Andrew Moore).

4.2.3 Difference from fourth delivery to prior deliveries

Finally, after receipt of the fourth map dataset, XOR comparisons were performed against the first, second, or third map datasets to detect changes from March 2023 to September 2024, from September 2023 to September 2024, or from March 2024 to September 2024. Three examples of changes are shown below.

Foliage changes in two different time windows are shown in Fig. 4.2.4.1. During the time window from March 2023 to September 2024 (left image), trees were cleared at the distribution center construction site, and so a change is visible (red arrow). This location shows little change during the time window from March 2024 to September 2024 (right image), since there was no further cutting and little foliage growth at this site.

Fig. 4.2.4.1 Left: Foliage differences from March 2023 (first delivery) to September 2024 (fourth delivery) across the entire 100 km^2 swath. Right: Foliage differences from March 2024 (third delivery) to September 2024 (fourth delivery). Since the tree clearing at the distribution center construction site occurred before March 2024, a foliage change is visible at left (red arrow) but not at right. there is no visible was collected Except the clear cut area (pink arrow) described above, differences are like due to organic growth. In both difference images, seasonal growth/trimming along Interstate 64 is evident (yellow arrow). *Left image feature sources: NASA from features ©2023, 2024 Maxar Technologies.*

Building demolition is revealed in a building difference map for the time window from March 2024 to September 2024, as shown in Figure 4.2.4.2. At left, 3D extruded XOR outputs for a street corner in Hampton Virginia shows a change to a set of buildings. Google Earth historical imagery at right confirms that a demolition occurred in this period.

As described in Section 3.3.2, the delivered lidar point were colorized cloud with the overhead image view. Without extensive processing, XOR differencing on point clouds is not feasible due to slight shifts between individual points between datasets. However, the results of an XOR on the vector layers can be used to guide manual verification of point cloud changes, as shown in Fig. 4.2.4.3. The two left images of Fig. 4.2.4.3 show the portion of the colorized point cloud from the third (April 2024) and fourth (September 2024) deliveries which is centered on a part of the NASA Langley Research Center. The vector layer XOR (not shown, but similar to Fig 4.2.1.1) highlighted a difference at the site (blue box) of new wind tunnel construction. The point cloud imagery shows that construction has just barely begun in April 2024, and is nearly complete in September 2024.

Fig. 4.2.4.2 Left: Building difference map for the time window from March 2024 to September 2024 shows a change on Von Schilling Drive in Hampton Virginia (76.3841494°W 37.0460990°N). Right: Google Earth historical imagery shows that building demolition occurred between November 2023 (top) and February 2024 (bottom).
Left image feature sources: NASA from features ©2024 Maxar Technologies. Left image base map sources: VGIN, Esri, TomTom, Garmin, SafeGraph, GeoTechnologies, Inc, METI/NASA, USGS, EPA, NPS, US Census Bureau, USDA, USFWS. Right image sources: Google Earth, Image 2025 © Airbus.

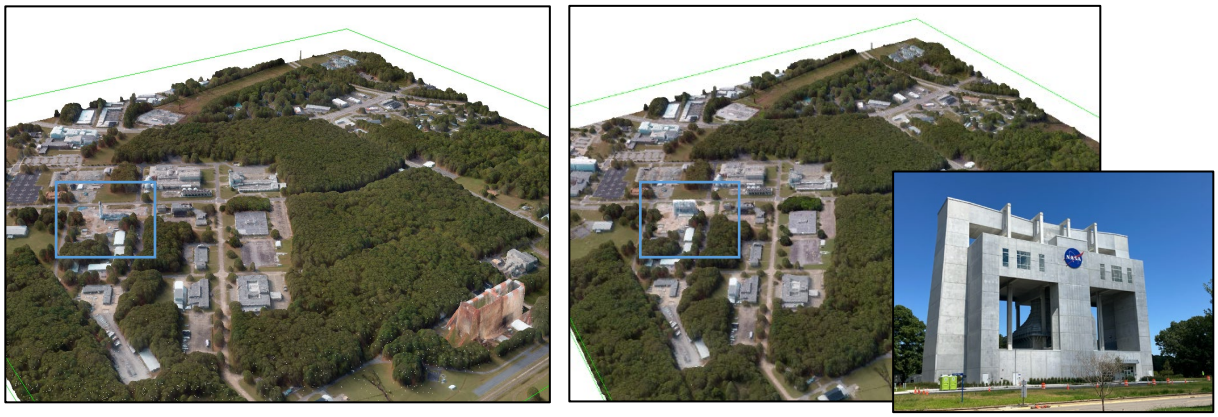

Fig. 4.2.4.3 Change detection on vector layer to verify change on point cloud layer. GPS coordinates from an XOR operation on building vector layers from the third and fourth deliveries were used to inspect the image overlay of the point cloud layer. Left: Section of point cloud from the third (April 2024) delivery showing new wind tunnel construction (blue box) at the NASA Langley Research Center. Right: The new wind tunnel is nearly complete in the terrain point cloud map from the fourth delivery (September 2024). Inset, right: The completed structure as of August 2025.
Map image source: ©2024 Maxar Technologies. Photo image sources: NASA (Corey Diebler).

5.0 Conclusion

This technical evaluation demonstrates that satellite-based photogrammetric mapping technology has matured to meet the accuracy and consistency requirements necessary for low-altitude aviation safety applications. The comprehensive assessment of four wide-area datasets spanning two years provides compelling evidence for the viability of this technology as an alternative to traditional aerial lidar surveys.

5.1 Key Findings

Accuracy Performance: Satellite-based 3D maps consistently met or exceeded specified accuracy requirements across all delivered data formats. Digital Terrain Model (DTM) data achieved the vendor-specified absolute accuracy of 3 m LE90/CE90 and relative accuracy of 1 m LE90/CE90. Vector representations of building features demonstrated typical edge placement accuracy of ±1 m, substantially better than the specified ±3 m requirement. The meter-level spatial resolution achieved is sufficient for identifying spatial hazards critical to low-altitude flight safety, including obstacle collision avoidance and emergency landing site characterization.

Temporal Consistency: Multi-temporal analysis across the four datasets revealed stable geometric representation of static terrain features, with appropriate detection and mapping of landscape changes due to construction and demolition activities. This temporal reliability is essential for maintaining current situational awareness in dynamic operational environments.

Data Management Advantages: The evaluation confirmed significant advantages in data storage and processing efficiency compared to traditional lidar approaches. Vector format geodata required only 100 MB of storage for the 100 km² study area, while point cloud format geodata required 8.5 GB. The 635 MB storage requirement for DTM data represents a manageable data volume for operational implementation.

5.2 Operational Implications and Limitations

The demonstrated capability of satellite-based mapping to deliver accurate, consistent terrain data at six-month intervals addresses key limitations of aerial lidar surveys, particularly regarding cost, scheduling flexibility, and data volume management. The continuous image acquisition capability of orbital satellite fleets offers potential for more frequent map updates than the current 56-day regulatory requirement, enhancing safety margins for emerging low-altitude operations.

However, operators must recognize the limitations of this technology. First, the 7 m × 7 m minimum feature resolution threshold means that smaller rooftop structures may not be consistently detected. Secondly – and far more critically – satellite-based maps cannot resolve very thin obstacles such as power lines present severe hazards to low-altitude flight operations. With high resolution aerial lidar (Fig. 5.2.1, top) power lines are resolvable [8], and even older lidar surveys with relatively low resolution can reveal the presence of this hazard, though with geometric gaps (Fig. 5.2.1, middle). Supplementary features such as a pseudo-obstacle geometric “shield” [20] (Fig. 5.2.1, bottom) along power line corridors could be prepared independently and added to wide-area satellite-based maps to compensate for this limitation.

5.3 Regulatory and Implementation Considerations

The validation results support the technical feasibility of satellite-based mapping for low-altitude aviation applications. The achieved accuracy levels meet the meter-level requirement for spatial hazard identification, and the temporal consistency demonstrates reliability for operational planning. However, regulatory acceptance for safety-critical applications will require continued validation and potential integration with complementary sensing technologies to address resolution limitations.

5.4 Future Work

Further development should focus on:

- extended temporal validation across longer time periods to confirm long-term stability,

- operational workflow development for automated change detection and map updating procedures,
- integration strategies with other sensing modalities to address thin obstacle detection limitations, and
- standardization of a power line corridor map representation to insert pseudo-obstacle such geometries such as the one shown in Fig. 5.2.1.

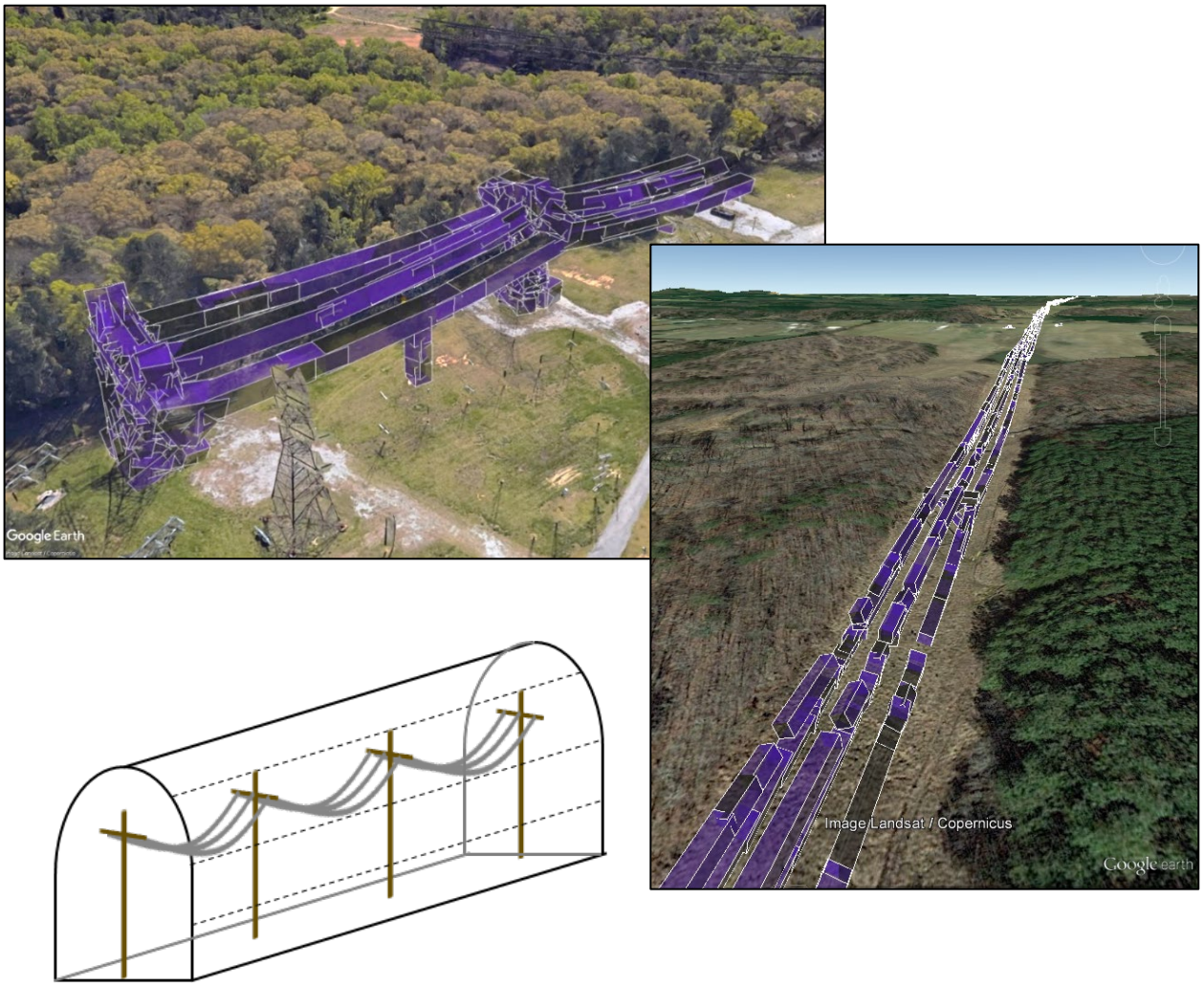

Fig. 5.2.1 A severe hazard not resolvable with current satellite-based terrain mapping: power lines. Shown here are two images from a prior lidar study [8]. Top: A section of a transmission line rendered with bounding boxes around points from an aerial lidar survey with an average point spacing of 0.33 m. Middle: The same rendering method applied to another transmission line surveyed with a coarser lidar sweep (0.6 m average point spacing). With a high resolution lidar survey, it is possible to construct a set of continuous geometries that form a “no fly zone” to avoid this hazard. Even the discontinuous “no fly” geometries of the lower resolution survey are preferable to no warning at all. Bottom: a virtual obstacle to enclose the towers and conductors [20].
© Lidar data: Dominion Energy; Left map image sources: Google and DigitalGlobe. Right map image sources: Google, Landsat/Copernicus and DigitalGlobe

5.5 Summary

This comprehensive two-year evaluation of satellite-based photogrammetric mapping technology demonstrates its readiness for low-altitude aviation safety applications. Through systematic assessment of four wide-area datasets covering the Virginia Peninsula region, the study validated that satellite photogrammetry consistently achieves the accuracy specifications required for aviation use: ±3m absolute and ±1m relative positioning accuracy for terrain features, with building edge placement typically within ±1m and never exceeding the ±3m threshold. The technology successfully detected structural changes over time, as demonstrated through building construction and demolition monitoring at NASA Langley Research Center and surrounding areas. While limitations exist in resolving small structures (<7m × 7m) and thin obstacles such as power lines—requiring complementary manual annotation—the satellite approach offers a viable and cost-effective alternative to traditional aerial lidar surveys for wide-area mapping applications. The validation against multiple reference sources, including high-precision lidar data from NASA Langley, confirms the technology's maturation to operational readiness for supporting safe low-altitude flight operations across large geographic areas.

References

[1] Federal Aviation Administration, “Order 7920.2, Notices in the Chart Supplement,” July 2, 2024, https://www.faa.gov/documentLibrary/media/Order/Order_7920.2_wApp.pdf, Accessed August 2025.

[2] Federal Aviation Administration, “Advisory Circular 150/5300-18B: General Guidance and Specifications for Submission of Aeronautical Surveys to NGS: Field Data Collection and Geographic Information System (GIS) Standards,” May 21, 2009, https://www.faa.gov/documentLibrary/media/Advisory_Circular/150-5300-18B-chg1-consolidated.pdf, Accessed August 2025.

[3] Young, Steven, Ersin Ancel, Andrew Moore, Evan Dill, Cuong Quach, John Foster, Kaveh Darafsheh et al. “Architecture and information requirements to assess and predict flight safety risks during highly autonomous urban flight operations.” NASA Technical Report, NASA-TM/2020-220440, January 2020.

[4] Ancel, Ersin, Andrew J. Moore, Steven D. Young, Evan T. Dill, Cuong Quach, and Kyle M. Smalling. "Testing a Run-Time Assurance Framework Coupled with Integrated Risk Mitigation Capabilities for Autonomous Urban UAS Flights." In *2024 AIAA DATC/IEEE 43rd Digital Avionics Systems Conference (DASC)*, pp. 1-9. IEEE, 2024.

[5] Tang, Matthew, John Thiel, and David Neckels. "System and methods for semi-automated editing of orthomosaics built from remotely-sensed imagery." U.S. Patent 10,474,895, issued November 12, 2019.

[6] Maxwell, Nicholas, John Papadakis, Adrian Ilie, S. Craig Stutts, Joseph Bates, and Benjamin L. Raskob. "Country-Scale Photogrammetry and True Orthorectification Using Very-High-Resolution (VHR) Multi-View Satellite Imagery." In IGARSS 2023-2023 IEEE International Geoscience and Remote Sensing Symposium, pp. 5607-5610. IEEE, 2023.

[7] Toutin, Thierry. "Review Article: Geometric processing of remote sensing images: models, algorithms and methods." International Journal of Remote Sensing 25, no. 10 (2004): pp. 1893-1924.

[8] Moore, Andrew, Matthew Schubert, Terry Fang, Joshua Smith, and Nicholas Rymer. "LiDAR-derived navigational geofences for low altitude flight operations." In AIAA AVIATION 2020 FORUM, p. 2908. 2020.
[9] Maxar Technologies, "About us," https://maxar.com/maxar-intelligence/about, Accessed August 2025.
[10] Moore, Laurence. "Transverse Mercator projections and us geological survey digital products." *U.S. Geological Survey, Professional Paper* (1997).
[11] Rydlund, Paul H., and Brenda K. Densmore. *Methods of practice and guidelines for using survey-grade global navigation satellite systems (GNSS) to establish vertical datum in the United States Geological Survey*. No. 11-D1. U.S. Geological Survey, 2012.
[12] Pavlis, Nikolaos K., Simon A. Holmes, Steve C. Kenyon, and John K. Factor. "The development and evaluation of the Earth Gravitational Model 2008 (EGM2008)." Journal of Geophysical Research: Solid Earth 117, no. B4 (2012).
[13] Maxar Technologies, “Precision3d Data Sheet Digital Terrain Model MXR-DS-DTM 01/22”, https://resources.maxar.com/data-sheets/precision3d-digital-terrain-model-dtm-data-sheet, Accessed January 2025.
[14] Maxar Technologies, “Precision3d Data Sheet Buildings MXR-DS-PRECISION3D 3/23”, https://resources.maxar.com/data-sheets/precision3d-buildings, Accessed January 2025.
[15] Maxar Technologies, “Precision3d Data Sheet Digital Surface Model MXR-DS-DSM 01/22”, https://resources.maxar.com/precision3d-data-suite/precision3d-digital-surface-model-dsm-data-sheet, Accessed January 2025.
[16] Maxar Technologies, “Precision3d Data Sheet Point Cloud MXR-DS-POINT CLOUD 01/22”, https://resources.maxar.com/precision3d-data-suite/precision3d-point-cloud-data-sheet, Accessed January 2025.
[17] Google, “Google Earth,” https://earth.google.com/about/, Accessed September 2025.
[18] ESRI, "Imagery (WGS84)," https://www.arcgis.com/home/item.html?id=52bdc7ab7fb044d98add148764eaa30a, Accessed September 2025.
[19] Microsoft Corporation, “Bing Maps,” https://www.bing.com/maps, Accessed September 2025.
[20] Moore, Andrew, Matthew Schubert, and Nicholas Rymer. "Autonomous inspection of electrical transmission structures with airborne UV sensors and automated air traffic management." In *2018 AIAA Information Systems-AIAA Infotech@ Aerospace*, p. 1628. 2018.
[21] U.S. Environmental Protection Agency, “About EPA,” https://www.epa.gov/aboutepa, Accessed September 2025.
[22] ESRI, “About ESRI,” https://www.esri.com/en-us/about/about-esri/company, Accessed September 2025.
[23] Garmin Ltd., “About us,” https://www.garmin.com/en-US/company/about-garmin/, Accessed September 2025.
[24] GeoTechnologies, Inc., “Our team,” https://www.geotechpa.com/team, Accessed September 2025.
[25] Jet Propulsion Laboratory, “ASTER Global Digital Elevation Map Announcement,” https://asterweb.jpl.nasa.gov/gdem.asp, Accessed September 2025.
[26] U.S. National Park Service, “About us,” https://www.nps.gov/aboutus/index.htm, Accessed September 2025.
[27] SafeGraph, “About us,” https://www.safegraph.com/about, Accessed September 2025.

[28] TomTom International, “About us,” https://www.tomtom.com/company/, Accessed September 2025.
[29] U.S. Census Bureau, “About the Bureau,” https://www.census.gov/about.html, Accessed September 2025.
[30] U.S. Department of Agriculture, “About USDA,” https://www.usda.gov/about-usda/general-information/our-agency, Accessed September 2025.
[31] U.S. Fish and Wildlife Service, “About us,” https://www.fws.gov/about, Accessed September 2025.
[32] U.S. Geological Survey, “About us,” https://www.usgs.gov/about/about-us, Accessed September 2025.
[33] Virginia Department of Emergency Management, “Virginia Geographic Information Network,” https://vgin.vdem.virginia.gov/, Accessed September 2025.

Appendix. Image source abbreviations

Abbreviation	Name	Reference
EPA	U.S. Environmental Protection Agency	[21]
Esri	Esri, Inc.	[22]
Garmin	Garmin Ltd.	[23]
GeoTechnologies, Inc.	GeoTechnologies, Inc.	[24]
METI/NASA	The Ministry of Economy, Trade, and Industry (METI) of Japan and the United States National Aeronautics and Space Administration (NASA)	[25]
NPS	U.S. National Park Service	[26]
SafeGraph	SafeGraph	[27]
TomTom	TomTom International	[28]
US Census Bureau	U.S. Census Bureau	[29]
USDA	U.S. Department of Agriculture	[30]
USFWS	U. S. Fish and Wildlife Service	[31]
USGS	U.S. Geological Survey	[32]
VGIN	Virginia Geographic Information Network	[33]